Structure, Conformations, and Repair of DNA Adducts from Dibenzo[*a,l*]pyrene: ^{32}P-Postlabeling and Fluorescence Studies

Ryszard Jankowiak,*[,†] Freek Ariese,[‡,||] Alan Hewer,[§] Andreas Luch,[▽,⊥] Dan Zamzow,[‡] Nicola C. Hughes,[§,#] David Phillips,[§] Albrecht Seidel,[▽] Karl-Ludwig Platt,[▽] Franz Oesch,[▽] and Gerald J. Small[†,‡]

Ames Laboratory−USDOE and Department of Chemistry, Iowa State University, Ames, Iowa 50011, Haddow Laboratories, Institute of Cancer Research, Sutton, Surrey SM2 5NG, U.K., and Institute of Toxicology, University of Mainz, D-55131 Mainz, Germany

Received December 23, 1997

The nature of stable DNA adducts derived from the very potent carcinogen dibenzo[*a,l*]pyrene (DB[*a,l*]P) in the presence of rat liver microsomes in vitro and in mouse skin in vivo has been studied using ^{32}P-postlabeling and laser-based fluorescence techniques. Analysis of DB[*a,l*]P−DNA adducts via ^{32}P-postlabeling has been obtained by comparison of the adduct patterns to those obtained from reactions of synthetic (±)-*anti*-, (+)-*anti*-, (−)-*anti*-, and (±)-*syn*-DB[*a,l*]P-11,12-diol 13,14-epoxide (DB[*a,l*]PDE) with single nucleotides and calf thymus DNA. *anti*-DB[*a,l*]PDE−dA adducts derived from the (−)-enantiomer are the major adducts formed in calf thymus DNA and in mouse skin DNA. The ratio of deoxyadenosine to deoxyguanosine modification is approximately 2:1 in mouse skin exposed to DB[*a,l*]P; activation by rat liver microsomes leads to a similar profile of adducts but with two additional spots. The conformations of DB[*a,l*]P adducts in native DNA, as well as the possibility of conformation-dependent repair, have been explored by low-temperature fluorescence spectroscopy. These studies have been performed using polynucleotides and calf thymus DNA reacted in vitro with DB[*a,l*]PDE and native DNA from mouse epidermis exposed to DB[*a,l*]P. The results show that adducts are heterogeneous, possess different structures, and adopt different conformations. External, external but base-stacked and intercalated adduct conformations are observed in calf thymus DNA and in mouse skin DNA samples. Differences in adduct repair rates are also revealed; namely, the analysis of mouse skin DNA samples obtained at 24 and 48 h after exposure to DB[*a,l*]P clearly shows that external adducts are repaired more efficiently than intercalated adducts. These results, taken together with those for B[*a*]P−DNA adducts [Suh et al. (1995) *Carcinogenesis* **16**, 2561−2569], indicate that the repair of DNA damage resulting from PAH diol epoxides is conformation-dependent.

Introduction

Dibenzo[*a,l*]pyrene (DB[*a,l*]P[1]) is a very potent carcinogen that requires enzymatic activation in biological systems to exhibit its biological activity via covalent DNA binding by electrophilic reactive metabolites (*1*−*9*). DB-[*a,l*]P belongs to a group of hexacyclic aromatic hydrocarbons that exhibit a range of carcinogenic activity on mouse skin (*1*, *7*, *8*) and in rat mammary gland (*1*, *7*). Dibenzopyrenes have been found to be present in tobacco smoke particulates (*10*), in coal tar, and in air, food, and water contaminated with combustion products (*11*). The carcinogenic activity of DB[*a,l*]P has been found to be significantly stronger than that of 7,12-dimethylbenz[*a*]-anthracene and benzo[*a*]pyrene (B[*a*]P), which were previously considered to be the most potent and widely studied carcinogenic polycyclic aromatic hydrocarbons (PAH) (*7*, *8*).

As revealed by adduct analysis in cell cultures, biotransformation of DB[*a,l*]P to DNA-binding metabolites results in the formation of fjord region *syn*- and *anti*-11,12-diol 13,14-epoxides (DB[*a,l*]PDE) (*4*−*6*), which have been reported to be extraordinarily strong mutagens and carcinogens (*12*−*15*). However, it appears that monooxygenation is not the exclusive pathway of metabolic activation of DB[*a,l*]P. On the basis of the analysis of DNA adducts produced after activation of DB[*a,l*]P in

* To whom correspondence should be addressed: Dr. Ryszard Jankowiak, Ames Laboratory−USDOE, Iowa State University, 706 Gilman Hall, Ames, IA 50011-3111. E-mail: jankowiak@ameslab.gov.
† Ames Laboratory−USDOE.
‡ Department of Chemistry.
§ Institute of Cancer Research.
▽ University of Mainz.
|| Present address: Institute for Environmental Studies, De Boelelaan 1115, NL-1081 HV Amsterdam, The Netherlands.
⊥ Present address: Technical University of Munich, Institute of Toxicology and Environmental Hygiene, Lazarettstr. 62, D-80636 Munich, Germany.
Present address: Division of Clinical Pharmacology and Toxicology, Hospital for Sick Children, Toronto, Ontario, Canada M5G 1X8.

[1] Abbreviations: CT, calf thymus; DB[*a,l*]P, dibenzo[*a,l*]pyrene; *anti*- and *syn*-DB[*a,l*]PDE, *anti*- and *syn*-dibenzo[*a,l*]pyrene-11,12-diol 13,-14-epoxide; DB[*a,l*]PDE-14-N7Ade, 14-(adenin-7-yl)-11,12,13-trihydroxy-11,12,13,14-tetrahydrodibenzo[*a,l*]pyrene; DB[*a,l*]PDE-14-N7Gua, 14-(guanin-7-yl)-11,12,13-trihydroxy-11,12,13,14-tetrahydrodibenzo-[*a,l*]pyrene; DB[*a,l*]P tetrol, 11,12,13,14-tetrahydroxy-11,12,13,14-tetrahydrodibenzo[*a,l*]pyrene; DE, diol epoxide; FLN, fluorescence line-narrowing; NLN, non-line-narrowing; PAH, polycyclic aromatic hydrocarbons; S_0 state, ground electronic state; S_1 state, lowest excited singlet state; TLC, thin-layer chromatography.

S0893-228x(97)00232-4 CCC: $15.00
Published on Web 05/13/1998

vitro by liver microsomes from 3-methylcholanthrene-induced rats, Li et al. reported that DB[*a*,*l*]P adduct formation also occurs by the one-electron oxidation metabolic pathway (*9*). Furthermore, Li et al. reported that the major DNA adducts formed in vitro by these two pathways are unstable due to rapid depurination reactions involving cleavage of the glycosidic bond. The relevance of apurinic sites is discussed in detail in refs *16* and *17*.

Analytical techniques which require digestion of DNA to the nucleotide level provide no insight on adduct conformation in the double-stranded helix. Nevertheless, adduct conformation is believed to play a major role in the biological effects of adducts, notably during replication and during DNA repair (*18*, *19*). In the case of B[*a*]P−DNA adducts, the repair rate in mouse skin was found to depend on adduct conformation, with intercalated and base-stacked external adducts being more persistent than adducts having an external conformation (*20*). The hypothesis that intercalated adducts are generally repaired less efficiently than helix-external adducts needs to be tested through experiments with other carcinogenic PAH.

Theoretical (*21*) and experimental (*22*) studies suggested that the same adduct is likely to adopt different conformations with different biological consequences. Geacintov (*23*, *24*) obtained evidence via linear dichroism studies which was most easily interpreted in terms of a single adduct giving rise to multiple conformations. NMR studies of the B[*a*]P-derived monooxygenation adducts also indicated the presence of multiple conformations (*24*). Loechler et al. (*25*, *26*) reported that B[*a*]P diol epoxide-derived adduct conformation is a key factor controlling the types of mutation at the lesion site. Various types of heterogeneity, i.e., due to structurally distinct and/or energetically inequivalent conformers, heterogeneity provided by an inhomogeneous environment of DNA, and polynucleotides have been discussed in ref *27*.

In the present study a comparative investigation of stable DNA adduct formation of DB[*a*,*l*]P in the presence of rat liver microsomes in vitro and in mouse skin in vivo has been undertaken using the ^{32}P-postlabeling and HPLC techniques. Analysis of DB[*a*,*l*]P−DNA adducts was performed by comparison of the adduct patterns with those obtained from reactions of synthetic (±)-*anti*-, (+)-*anti*-, (−)-*anti*-, and (±)-*syn*-DB[*a*,*l*]PDE with single nucleotides and calf thymus (CT)-DNA. The chemical structures of the fjord region diol epoxides of DB[*a*,*l*]P are shown in Figure 1. The conformations of DB[*a*,*l*]P−DNA adducts and the possibility of conformation-dependent repair have been explored by low-temperature fluorescence spectroscopy. Fluorescence measurements have been performed using polynucleotides and CT-DNA reacted in vitro with DB[*a*,*l*]PDE, and native DNA from mouse skin exposed to DB[*a*,*l*]P.

This study provides direct comparison of two different approaches for DNA adduct analysis, i.e., ^{32}P-postlabeling HPLC and low-temperature fluorescence spectroscopy, and shows that both methods not only complement each other but also provide consistent results. In addition to the characterization and quantitation of adducts at the nucleotide level by the ^{32}P-postlabeling approach, low-temperature laser-excited fluorescence methods allow for differentiation between various conformations of DB[*a*,*l*]P adducts in native DNA and reveal differences in their repair rates in mouse skin exposed to DB[*a*,*l*]P. Thus, the results presented here support our earlier findings (*20*) that adduct repair is conformation-dependent.

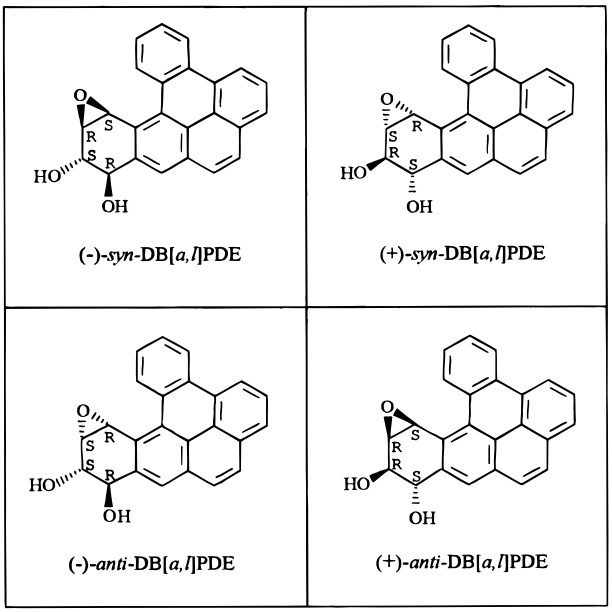

Figure 1. Structures of the four possible fjord region diol epoxides of dibenzo[*a*,*l*]pyrene. In the present study, optically active (+)-*anti*-(11*S*,12*R*,13*R*,14*S*)- and (−)-*anti*-(11*R*,12*S*,13*S*,14*R*)-diol epoxides and a racemic mixture of the (+)- and (−)-*syn*-(11*R*,12*S*,13*R*,14*S*)-diol epoxides were used.

Materials and Methods

Caution: *DB[a,l]P and DB[a,l]PDE are hazardous chemicals; they should be handled in accordance with NIH guidelines.*

Adduct Formation with CT-DNA, Polyoligonucleotides, and Nucleoside 3′-Monophosphates of Deoxynucleoside 3′-Monophosphates. Poly(dG)•poly(dC) or poly(dA)•poly(dT) (0.1 μg/μL), nucleoside 3′-monophosphate of deoxyribonucleoside 3′-monophosphates (0.1 μg/μL), or CT-DNA (2.0 μg/μL) in 0.1 M Tris-HCl buffer (pH 7.4, 500 μL total volume) was mixed with 50 μg (0.142 μmol) of *syn*- or *anti*-diol epoxide dissolved in 50 μL of dimethyl sulfoxide. After incubation at 37 °C for 4 h the reaction mixture was extracted with 500 μL of water-saturated ethyl acetate (three times) and subsequently with 500 μL of water-saturated diethyl ether (twice) to remove excess of unreacted diol epoxide and/or its hydrolysis products. The extraction mixture was efficiently separated each time by centrifugation (13 000 rpm). In the case of the modified oligonucleotides and CT-DNA, ethanol (2 volumes) and NaCl (5 M, 0.1 volume) were subsequently added to the solution, which was then kept overnight at −20 °C to complete the precipitation. The modified oligonucleotide or CT-DNA, separated by centrifugation for 30 min (13 000 rpm), was rinsed with aqueous ethanol (70%), centrifuged again, and dried under vacuum. In experiments with modified nucleotide 3′-monophosphates of deoxyribonucleoside 3′-monophosphates, the aqueous phase was used directly without further precipitation. Denaturation of adducted poly(dA)•poly(dT) in buffer solution was obtained via heating to ∼90 °C and rapid cooling to either 77 or 4.2 K.

DB[*a*,*l*]P-Modified DNA from Incubations with Rat Liver Microsomal Fractions. Rat hepatic microsomal fractions were prepared from 3-methylcholanthrene-treated animals using the method described by Tierney et al. (*28*). DB[*a*,*l*]P (0.1 μmol) was incubated with the microsomal preparation in the presence of cofactors and DNA, as described by Hughes and Phillips (*29*).

DB[*a*,*l*]P-Modified DNA from Mouse Skin. Groups of four male Parkes mice (6−8 weeks old) purchased from the MRC

National Institute for Medical Research (Mill Hill, London, U.K.) were treated with DB[*a*,*l*]P; 1 μmol in 200 μL of acetone per mouse was applied to shaved areas of their backs. Control animals received acetone only. Groups of four animals were killed by cervical dislocation at 24 and 48 h after treatment. Treated areas of the skin were removed and frozen; DNA was isolated as described by Hughes and Phillips (*3*, *29*).

^{32}P-Postlabeling. DNA from mouse skin and from incubations with rat liver microsomal preparations was digested enzymatically and ^{32}P-postlabeled using the nuclease P_1 digestion procedure to enhance the sensitivity of the assay, as described previously (*3*). DNA and 3′-mononucleotides that had been reacted with DB[*a*,*l*]P diol epoxides were analyzed using the standard ^{32}P-postlabeling procedure (*30*). Resolution of the ^{32}P-labeled adducts was carried out on 10- × 10-cm poly(ethylenimine) cellulose TLC plates using solvent system I described previously (*29*): D1, 1.0 M sodium phosphate (pH 6.0); D2, 3.5 M lithium formate, 8.5 M urea (pH 3.5); D3, 0.8 M lithium chloride, 0.5 M Tris-HCl, 8.5 M urea (pH 8.0); D4, 1.7 M sodium phosphate (pH 6.0). To improve resolution of the adduct spots, solvents D2 and D3 were run onto short paper wicks (4 cm in length), in addition to the usual procedure which also involves running solvents D1 and D4 onto wicks.

HLPC Analysis. After quantitation on TLC, adduct spots were eluted with pyridinium formate (4 M, pH 4.5, 500 μL) overnight and the eluates filtered and evaporated to dryness. The residues were redissolved in deionized water (100 μL) before injection onto a Zorbax phenyl-modified reverse-phase column (250 × 4.6 mm; particle size, 5 μm). Elution was with the following solvent system: 0−15 min, a linear gradient of 10−46% buffer B (methanol−buffer A, 9:1) in buffer A (the composition of buffer A was 0.3 M sodium dihydrogen orthophosphate and 0.2 M orthophosphoric acid, adjusted to pH 2.0); 15−60 min, a linear gradient of 46−48% B in buffer A; 60−80 min, a linear gradient of 48−80% B in buffer A, all at a flow rate of 1.2 mL/min. Phenanthrene-9,10-diol was used as an internal marker, with a retention time of approximately 40 min (*31*).

Low-Temperature Fluorescence Spectroscopy. A detailed description of the apparatus used for fluorescence line-narrowing (FLN) and non-line-narrowing (NLN) spectroscopy is given elsewhere (*32*). Briefly, the excitation source was a Lambda Physik FL-2002 dye laser pumped by a Lambda Physik EMG 102 MSC XeCl excimer laser. The cryostat was a double-nested glass Dewar fitted with quartz optical windows. For gated detection of fluorescence signals, the output of a reference photodiode was used to trigger a high-voltage gate pulse generator to define the temporal observation window of a Princeton Instruments IRY 1024/G/B intensified photodiode array. Various delay times and gate widths were utilized (see figure captions). A 1-m focal length McPherson 2061 monochromator was used to disperse the fluorescence. For high-resolution measurements the monochromator was equipped with a 2400 grooves/mm grating, providing an 8-nm spectral window. FLN spectra were acquired using many different laser excitation wavelengths, each revealing a portion of the S_1 excited-state vibrational frequencies of the analyte. Low-resolution NLN fluorescence spectra were recorded using the same monochromator fitted with a 150 grooves/mm grating, yielding a 160-nm window. Various laser excitation wavelengths and different observation windows (i.e., detector delay times) were used to reveal adduct heterogeneity; only selected spectra are shown below.

All samples were studied in aqueous buffer to mimic the situation in a cellular environment (*30*). DNA samples were dissolved in 30−40 μL of 20 mM sodium phosphate buffer (pH 7.0; 100 mM NaCl), and the resulting solutions (DNA concentration ∼3 mM in base pairs) were transferred to quartz tubes for spectroscopic analysis at 77 and 4.2 K. Ethanol-precipitated solid pellets of mouse skin DNA were also analyzed for comparison. Synthesized polynucleotide−DB[*a*,*l*]PDE samples were dissolved in 30 μL of 20 mM sodium phosphate buffer. To eliminate any dependence on cooling rate (*34*), samples were kept on ice for at least 20 min before rapid cooling in liquid helium (for FLN) or liquid nitrogen (for NLN fluorescence measurements).

Results

^{32}P-Postlabeling. 1. DNA Adducts in Mouse Skin. ^{32}P-Postlabeling analysis of DNA isolated from the skin of mice that had been topically treated with DB[*a*,*l*]P is shown in Figure 2B. The chromatogram reveals the presence of three major adducts (spots 1−3) and four minor adducts (spots 4−7). The pattern of adduct spots is essentially the same for DNA samples isolated at 24 and 48 h after treatment. The total adduct level at 24 h is 63.1 fmol/μg of DNA (2082 adducts/10^8 3′-nucleotides) and at 48 h is 46 fmol/μg of DNA (1518 adducts/10^8 3-′nucleotides) (*3*). The relative amounts of radioactivity in each adduct spot for DNA isolated at 24 h are given in Table 1.

2. DNA Adducts from Rat Liver Microsomal Incubations. The pattern of adducts obtained with DNA that had been incubated with DB[*a*,*l*]P and rat liver microsomal fractions is shown in Figure 2A. The same seven adducts seen in mouse skin are observed (spots 1−7), with two additional minor spots (8 and 9). The relative amounts of radioactivity in each spot are given in Table 1.

Adducts Formed by Diol Epoxides Reacted with DNA and Mononucleotides. 1. (−)-*anti*-DB[*a*,*l*]-PDE. The products of the reaction of this diol epoxide with DNA, dGp, and dAp are shown in Figure 2C,D,E, respectively. Three major adducts (spots 1−3) and two minor adducts (spots 5 and 6) are formed with DNA. By comparing the patterns of adduct spots in Figure 2C−E, it is clear that two of the adducts formed in the reaction of this diol epoxide with DNA involve modification of guanine (spots 1 and 5) and three are adenine adducts (spots 2, 3, and 6). An extra spot (spot 10, Figure 2E) is observed only for the reaction with dAp.

2. (+)-*anti*-DB[*a*,*l*]PDE. Four major adducts (spots 2 and 11−13) and three minor adducts (spots 14−16) are formed with DNA, as shown in Figure 2F. Of these, two involve modification of guanine (spots 11 and 12; compare with Figure 2G), and three are adenine adducts (spots 13−15; compare with Figure 2H). Two extra spots (spots 2 and 16) are observed only for the reaction of this diol epoxide with DNA, leading to the possible conclusion that they involve reaction with cytosine.

3. (±)-*syn*-DB[*a*,*l*]PDE. As shown in Figure 2I, (±)-*syn*-DB[*a*,*l*]PDE forms four major adducts (spots 1*, 4, 7, and 8) and three minor adducts (spots 17−19) with DNA. Of these, two involve reaction with guanine (spots 8 and 17; compare with Figure 2J), and four involve reaction with adenine (spots 1*, 4, 7, and 19; compare with Figure 2K). A minor adduct (spot 18) is observed only for the reaction of this diol epoxide with DNA, suggesting that it is possibly a cytosine adduct. The relative intensities of all the adduct spots formed by diol epoxides reacted with DNA and 3′-mononucleotides are summarized in Table 1.

Identification of Adducts Formed in Mouse Skin and Rat Liver Microsomal Incubations. 1. Thin-Layer Chromatography. The results of the ^{32}P-postlabeling experiments are summarized in Table 2, where the adduct patterns observed for DNA isolated from mouse skin and rat liver microsomes are compared to

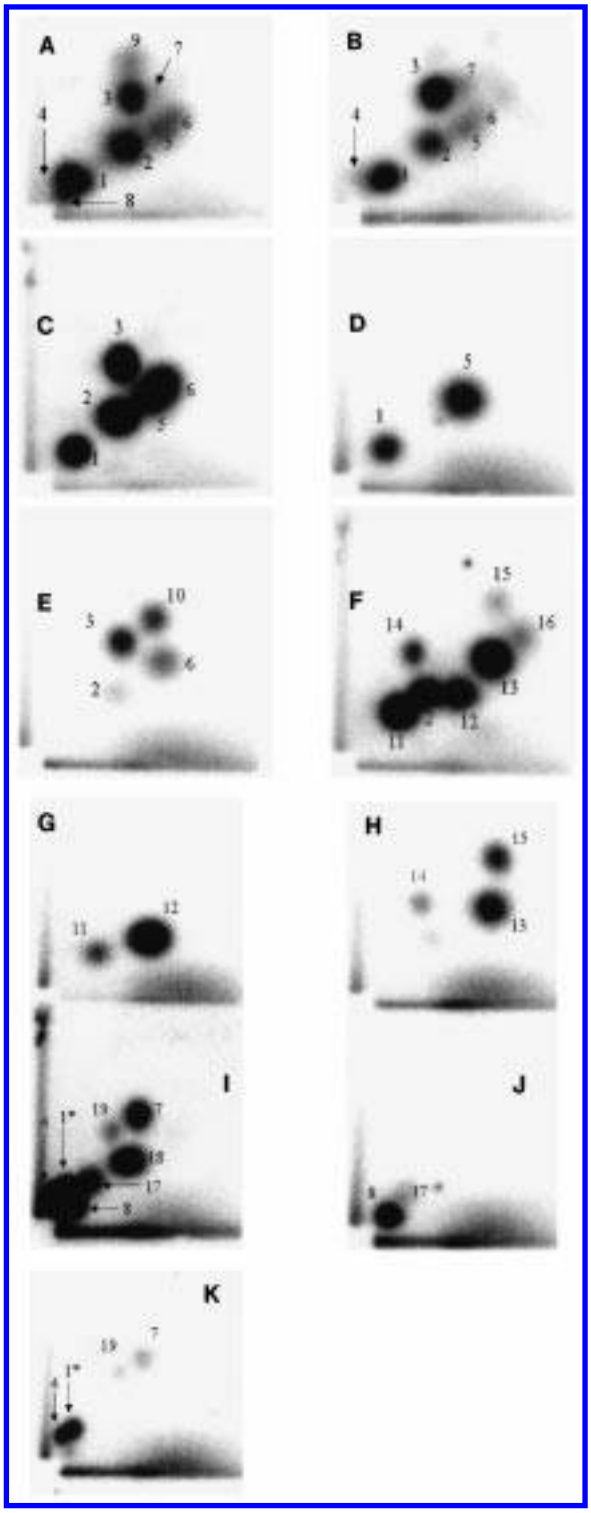

Figure 2. ^{32}P-Postlabeling autoradiographs of DB[*a*,*l*]PDE adducts from (A) DNA from rat liver microsomal incubations with DB[*a*,*l*]P in vitro; (B) mouse skin DNA exposed (24 h) to DB[*a*,*l*]P in vivo; (−)-*anti*-DB[*a*,*l*]PDE reacted with DNA (C), with dGp (D), and with dAp (E); (+)-*anti*-DB[*a*,*l*]PDE reacted with DNA (F), with dGp (G), and with dAp (H); (±)-*syn*-DB[*a*,*l*]-PDE reacted with DNA (I), with dGp (J), and with dAp (K).

those obtained by reaction of the diol epoxides with DNA and 3′-mononucleotides. In mouse skin exposed to DB-[*a*,*l*]P, seven adducts (spots 1−7) are observed: five of the seven adducts in mouse skin are formed by (−)-*anti*-DB[*a*,*l*]PDE (spots 1−3, 5, and 6 in Figure 2A), and two minor adducts are formed by (±)-*syn*-DB[*a*,*l*]PDE (spots 4 and 7). One major adduct (spot 1) and one minor adduct (spot 5) are formed with guanine residues, and the rest involve modification of adenine. Thus the ratio of guanine to adenine modification (for the DNA samples obtained after 24 h and the dose of DB[*a*,*l*]P used) is approximately 1:2 in mouse skin exposed to DB[*a*,*l*]P. The activation of DB[*a*,*l*]P by rat liver microsomes leads to a similar profile of adducts, but with two extra spots (8 and 9 in Figure 2B). Adduct spot 8 results from the reaction of (±)-*syn*-DB[*a*,*l*]PDE with guanine residues. Adduct spot 9 did not comigrate with any of the synthetic adducts; its identity is therefore unknown.

Adduct spot 1 in the mouse skin and rat liver microsome experiments, which appears to consist primarily of a (−)-*anti*-DB[*a*,*l*]PDE adduct with guanine, may also

Table 1. ^{32}P-Postlabeling Analysis of DB[*a*,*l*]P−DNA Samples Isolated at 24 h

sample	adduct spot number[a]	total radioactivity (%)
DNA from mouse skin exposed to DB[*a*,*l*]P[b] (Figure 2B)	1	25.7 ± 2.1
	2	28.1 ± 9.5
	3	32.8 ± 5.0
	4	1.6 ± 0.7
	5	7.2 ± 0.2
	6	3.3 ± 0.3
	7	1.4 ± 1.6
DNA from rat liver microsomal incubations with DB[*a*,*l*]P[b] (Figure 2A)	1 + 4 + 8	36.8 ± 1.3
	2	27.4 ± 3.2
	3	17.9 ± 3.7
	5 + 6	14.8 ± 1.9
	7	0.9 ± 1.0
	9	2.3 ± 2.5
(−)-*anti*-DB[*a*,*l*]PDE and CT-DNA (Figure 2C)	1	16.6
	2	30.6
	3	24.7
	5 + 6	28.0
(−)-*anti*-DB[*a*,*l*]PDE and dGp (Figure 2D)	1	30.9
	5	69.1
(−)-*anti*-DB[*a*,*l*]PDE and dAp (Figure 2E)	2	6.5
	3	40.6
	6	25.9
	10	27.0
(+)-*anti*-DB[*a*,*l*]PDE and CT-DNA (Figure 2F)	2	17.9
	11	29.2
	12	14.4
	13	30.1
	14	4.3
	15	1.3
	16	2.8
(+)-*anti*-DB[*a*,*l*]PDE and dGp (Figure 2G)	11	13.3
	12	86.7
(+)-*anti*-DB[*a*,*l*]PDE and dAp (Figure 2H)	13	62.3
	14	7.7
	15	30.0
(±)-*syn*-DB[*a*,*l*]PDE and CT-DNA (Figure 2I)	1*	8.7
	4	10.2
	7	9.0
	8	50.7
	17	6.8
	18	12.6
	19	1.9
(±)-*syn*-DB[*a*,*l*]PDE and dGp (Figure 2J)	8	86.7
	17	13.3
(±)-*syn*-DB[*a*,*l*]PDE and dAp (Figure 2K)	1*	42.1
	4	45.9
	7	8.2
	19	3.8

[a] As shown in Figure 2. [b] The mean ± standard deviation of four determinations.

Table 2. DB[*a*,*l*]P−DNA Adducts from Mouse Skin, Rat Liver Microsomal Incubations, and Chemical Reactions

adduct number	(−)-*anti*-DE/DNA	(+)-*anti*-DE/DNA	(±)-*syn*-DE/DNA	(−)-*anti*-DE/dGp	(+)-*anti*-DE/dGp	(±)-*syn*-DE/dGp	(−)-*anti*-DE/dAp	(+)-*anti*-DE/dAp	(±)-*syn*-DE/dAp
1/1[a]	√		√[a]	√					√[a]
2	√	√[b]					√		
3	√						√		
4			√						√
5	√			√					
6	√						√		
7			√						√
8[c]			√			√			
9[c]									

[a] A minor spot from (±)-*syn*-DB[*a*,*l*]PDE/dAp comigrates with a major spot from (−)-*anti*-DB[*a*,*l*]PDE/dGp. [b] (+)-*anti*-DB[*a*,*l*]PDE/DNA gives a minor spot that comigrates with spot 2, but (+)-*anti*-DB[*a*,*l*]PDE did not give this spot with either dGp or dAp. Therefore, this (+)-*anti*-DB[*a*,*l*]PDE/DNA adduct may involve modification of cytosine. [c] These adducts form in DNA from rat liver microsomal incubations, but not in mouse skin. Adduct 9 did not comigrate with any of the synthetic adducts formed from reactions of these diol epoxides with DNA, dAp, or dGp.

Table 3. Retention Times on HPLC of Adduct Spots Eluted from TLC

	retention time (min)				
adduct spot	mouse skin (A)	microsomal incubation (B)	in vitro adduct (C)	A + C coinjected	B + C coinjected
1	48	44	45	45	44
2	21, 55	21, 55, 61	59, 74	50, 70	−
3	73	74	71	71	71
4	−	−	−	−	−
5	34	34	34	34	34
6	49	42	42	−	42
7	−	−	−	−	−

contain a minor contribution from a (±)-*syn*-DB[*a*,*l*]PDE adduct with adenine (spot 1* in Figure 2K). In addition, adduct spot 2, which is primarily due to a (−)-*anti*-DB[*a*,*l*]PDE adduct with adenine, may also contain a component resulting from the reaction of (+)-*anti*-DB[*a*,*l*]PDE with DNA that is not formed with dGp or dAp.

HPLC. To confirm the adduct designations made on the basis of TLC mobility, adduct spots were excised and the radioactivity was eluted and further chromatographed on HPLC. The results are summarized in Table 3. Adduct spot 1 from mouse skin (Figure 2B) gave a single peak with a retention time between 45 and 50 min (Table 3). Adduct 1 from the reaction of (−)-*anti*-DB[*a*,*l*]PDE with dGp (Figure 2D) also gave a single peak with similar retention time; when coinjected on to HPLC, the two products gave a single radioactive peak. Adduct 1 from the microsomal incubations (Figure 2A) also gave a peak at this retention time that coeluted with adduct 1 from the reaction of (−)-*anti*-DB[*a*,*l*]PDE with dGp, but it also gave other radioactive peaks between 20 and 30 min. Similar analyses of adduct 3 from skin, microsomal incubation and in vitro reaction (Figure 2B,A,E, respectively) gave in each case a single peak eluting at between 71 and 74 min; coinjection resulted in radioactivity coeluting as a single peak in each case (chromatograms not shown). For adduct 5 (Figure 2A,B,D), single peaks of radioactivity at 34 min were obtained in each case, and these coeluted with each other when coinjected onto HPLC. For adduct 6 (Figure 2A,B,E), the same result was obtained with the adduct from microsomal incubations and the corresponding in vitro adduct (retention time 42 min), but insufficient radioactivity was obtained from mouse skin DNA to perform satisfactory coinjection experiments, even though this material eluted as a single peak with a similar retention time.

However, the results with adduct spot 2 (Figure 2A,B,E) displayed greater complexity. HPLC analysis resulted in the elution of several peaks; in each of the three cases there was a peak eluting between 55 and 61 min; for mouse skin DNA and microsomal incubations another peak was seen at 21 min, and for the in vitro reaction product [from the reaction of (−)-*anti*-DB[*a*,*l*]-PDE with dAp] there was an additional major peak at 74 min. Coinjection experiments revealed that the mouse skin and in vitro peaks between 50 and 60 min coeluted. Insufficient radioactivity was eluted from spots 4 and 7 to permit further analysis on HPLC.

Low-Temperature Fluorescence Spectroscopy. In this section DNA adducts are assessed by laser-induced fluorescence spectroscopy, performed under line-narrowing (at 4.2 K) and non-line-narrowing ($S_2 \leftarrow S_0$ laser excitation at $T = 77$ K) conditions. Various excitation wavelengths were used; only selected spectra are presented. It is shown below that time-resolved spectroscopy and selective laser excitation provide a means for structural adduct assignment. The data shown establish that DB[*a*,*l*]PDE-derived DNA adducts exist in multiple conformations.

1. External versus Intercalated Adduct Conformations. DB[*a*,*l*]P adducts having their fluorescence origin band at wavelengths shorter or longer than 395 nm are labeled as external and intercalated, respectively (see Discussion section). The presence of different adduct conformations is demonstrated in Figure 3 by NLN fluorescence spectra of (±)-*anti*-DB[*a*,*l*]PDE−poly(dA)•poly(dT) adducts before (spectrum a) and after (spectrum b) denaturing the sample. The (0,0) band of the major adduct of (±)-*anti*-DB[*a*,*l*]PDE−poly(dA)•poly(dT) is located at 398 nm (curve a). Upon denaturation to the single-stranded polynucleotide, the origin band shifts to 382.6 nm (curve b). Similar spectra were observed for the (−)-*anti*-DB[*a*,*l*]PDE−poly(dA)•poly(dT) adducts (spectra not shown). The FLN spectrum obtained for the denatured sample (curve c, Figure 3) is different from FLN spectra obtained for tetrols derived from *anti*-DB[*a*,*l*]PDE (*35*). The spectra were also different from the FLN spectra obtained for the physical complexes of DB[*a*,*l*]P tetrols with DNA (data not shown). This indicates that the origin band at 382.6 nm does not correspond to

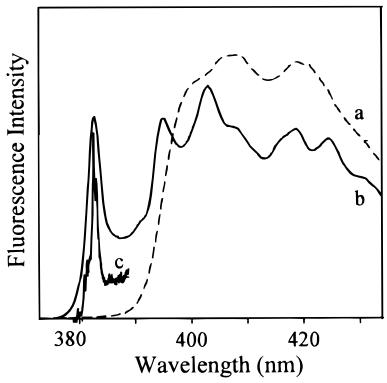

Figure 3. NLN fluorescence spectra of *anti*-DB[*a*,*l*]PDE−poly(dA)•poly(dT) before (spectrum a) and after (spectrum b) denaturing the oligonucleotide. Both spectra were obtained for λ_{ex} = 360 nm at T = 77 K. The FLN spectrum (curve c; λ_{ex} = 372 nm, T = 4.2 K) of *anti*-DB[*a*,*l*]PDE−poly(dA) is different from the FLN spectra of DB[*a*,*l*]P tetrols (tetrol spectra not shown).

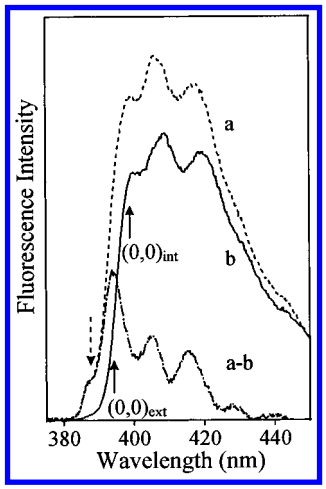

Figure 4. NLN fluorescence spectra (T = 77 K) of adducts from (±)-*anti*-DB[*a*,*l*]PDE bound to poly(dG)•poly(dC). Spectra a and b were obtained at 50-ns delay time for λ_{ex} = 308 and 360 nm, respectively. The $(0,0)_{int}$ origin band is located at ∼398 nm. The difference spectrum (a − b) shows the existence of an adduct fraction with more helix-external character and (0,0) band at 394.2 nm.

hydrolysis products but to a dA adduct. Thus the two fluorescence origin bands at 382.6 and 398 nm are most likely associated with different conformations of the same adduct in different DNA conformations, external and intercalated, respectively.

2. (±)-*anti*-DB[*a*,*l*]PDE Adducts with Polynucleotides. NLN fluorescence spectra for adducts resulting from binding of (±)-*anti*-DB[*a*,*l*]PDE to poly(dG)•poly(dC) are shown in Figure 4. Curves a and b were obtained for two different excitation wavelengths, but otherwise identical conditions. Spectrum a was obtained with 308-nm excitation. This wavelength has poor selectivity that excites both external and intercalated conformations (*20*) and reveals the fluorescence emission from all adducts. The weak peak indicated by the dashed arrow is most likely due to a tetrol hydrolysis product (*35*). Spectrum b was obtained with excitation at 360 nm; data obtained for different excitation wavelengths revealed that the 360-nm wavelength excites more selectively the intercalated adducts. Apparently, the intercalated adducts must have much stronger absorption extinction coefficient (in that region) than the external adduct types. The resulting fluorescence (0,0) band is located at 398 nm. The

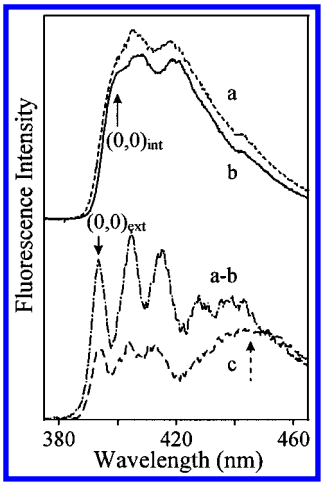

Figure 5. NLN fluorescence spectra (T = 77 K) of adducts from (±)-*anti*-DB[*a*,*l*]PDE bound to poly(dA)•poly(dT). Spectra a and b were obtained for λ_{ex} = 308 and 360 nm, respectively, and a 50-ns delay time. The spectrum a − b is the difference between spectra a and b, while curve c is a temporal difference spectrum between spectra acquired at 0- and 50-ns delay times with λ_{ex} = 360 nm.

difference spectrum (a − b) shows the existence of an adduct fraction having more helix-external character and a blue-shifted emission maximum at 394.2 nm. All of these spectra show the characteristic vibronic progression of benzo[*e*]pyrene, the fluorescent chromophore (*35*, *36*). The contribution from the external adducts could also be revealed by exploiting differences in fluorescence lifetimes of the external and intercalated adducts. A spectrum very similar to the difference spectrum (a − b) in Figure 4 was obtained as the difference between spectra obtained at 0- and 50-ns delay times for λ_{ex} = 360 nm (data not shown). This was possible because, as established in the course of this work, the external adduct type has a shorter fluorescence lifetime than the intercalated adducts (∼80 versus ∼130 ns), and therefore, when using a shorter detector delay time, a larger contribution from this conformational subpopulation was revealed. Other examples of this procedure will be shown below. Since (±)-*anti*-DB[*a*,*l*]PDE has been shown to react predominantly with purine bases (*4*−*6*, *9*, *33*, *37*), it is reasonable to assume that the adducts formed with poly(dG)•poly(dC) correspond to dG adducts formed via either cis or trans opening of the epoxide (see Discussion).

The spectroscopic characteristics of DB[*a*,*l*]PDE−adenine adducts obtained from the reaction of (±)-*anti*-DB[*a*,*l*]PDE with poly(dA)•poly(dT) are shown in Figure 5. Spectra a and b were acquired with excitation wavelengths of 308 and 360 nm, respectively. Again, the difference spectrum (a − b) reveals the contribution from helix-external adducts, but this contribution is much weaker than that observed in Figure 4 for poly(dG)•poly(dC). The external (±)-*anti*-DB[*a*,*l*]PDE−poly(dA)•poly(dT) adducts possess a shorter fluorescence lifetime compared to the intercalated adducts, so the external adduct fraction can also be revealed via time-resolved spectroscopy. This is shown in Figure 5c, which is the spectrum obtained as the difference between spectra measured using two different detector delay times (0 and 50 ns), but the same laser wavelength (360 nm). Similar results were obtained for 308-nm excitation. The temporal difference spectrum (c) reveals the spectrum of the component having the shorter fluorescent lifetime, the external adduct conformation. Note that the difference

Table 4. Summary of Adduct Conformations, Based on Low-Temperature Fluorescence Spectra, Formed in Duplex Polynucleotides and DNA in Vitro from Reaction with (±)-*anti*- and (±)-*syn*-DB[*a,l*]PDE

	(±)-*anti*-DB[*a,l*]PDE			(±)-*syn*-DB[*a,l*]PDE		
sample	adduct label	(0,0) band (nm)	conformation assignment	adduct label	(0,0) in (nm)	conformation assignment
poly(dG)•poly(dC)[a]	–			(±)-1	382.5	*syn*-dG_{ext}[b]
	(±)-2	394.2	*anti*-dG_{ext}	(±)-2	392.6	*syn*-dG_{ext}[b]
	(±)-3	398	*anti*-dG_{int}	(±)-3	399	*syn*-dG_{int}
poly(dA)•poly(dT)	(±)-2	393.4	*cis-anti*-dA_{ext}	(±)-2	392.5	*syn*-dA_{ext}
	(±)-3	398	*anti*-dA_{int}	(±)-3	399	*syn*-dA_{int}
	c	445	two *anti*-dA_{ext} on neighboring bases	*c*	440	two *syn*-dA_{ext} on neighboring bases
CT-DNA	(±)-2	394.2	*anti*-dG_{ext} and *anti*-dA_{ext}	(±)-2	392.6	*syn*-dG_{ext} and *syn*-dA_{ext}
	(±)-3	398	*anti*-dG_{int} and/or *anti*-dA_{int}	(±)-3	399	*syn*-dA_{int} and/or *syn*-dG_{int}
	c	445	two *anti*-dA_{ext} (a minor contribution)	*c*	440	two *syn*-dA_{ext} (a large contribution)

[a] No excimer fluorescence was observed for the poly(dG)•poly(dC) samples. [b] These two external adducts likely have similar conformations of the cyclohexenyl ring but different DNA base-stacking interactions. [c] External adducts bound to neighboring or closely spaced adenine bases, as revealed by excimer-type fluorescence.

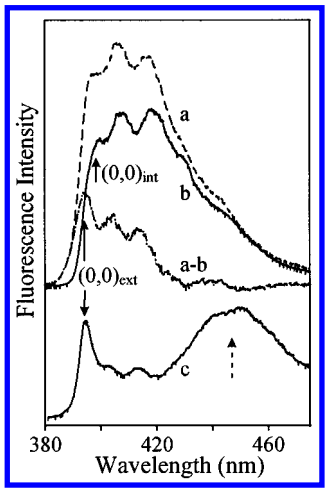

Figure 6. Fluorescence spectra of adducts from the in vitro reaction of (±)-*anti*-DB[*a,l*]PDE with CT-DNA, obtained for λ_{ex} = 308 nm and 50-ns delay time (spectrum a) and for λ_{ex} = 360 nm and 100-ns delay (spectrum b). Spectrum a − b is the difference between spectra a and b. Spectrum c is the temporal difference spectrum for two fluorescence spectra obtained at different detector delay times, 0 and 50 ns.

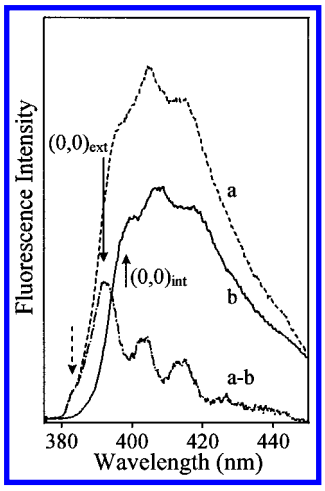

Figure 7. NLN spectra of (±)-*syn*-DB[*a,l*]PDE adducts in a double-stranded poly(dG)•poly(dC) oligonucleotide; T = 77 K. Spectrum a was obtained using nonselective excitation at 308 nm, while spectrum b was obtained using selective excitation of intercalated adducts at 370 nm. The difference spectrum a − b reveals the adduct fraction having an external conformation with (0,0) band at 392.6 nm [(±)-2]. A minor contribution from another adduct with an even more external character is observed at 382.5 nm [(±)-1].

spectrum (c) also reveals a broad band at 445 nm. This band, observed only at very short delay times, corresponds to excimer type fluorescence which was not observed for the poly(dG)•poly(dC) oligonucleotide samples (see Table 4).

3. (±)-*anti*-DB[*a,l*]PDE Adducts with DNA. Fluorescence spectra of adducts resulting from the reaction of (±)-*anti*-DB[*a,l*]PDE with CT-DNA are shown in Figure 6. Comparison of spectrum a, acquired using nonselective excitation at 308 nm, and spectrum b, acquired using more selective excitation at 360 nm, also indicates the presence of at least two adduct conformations. In addition to intercalated adducts having a red-shifted fluorescence (0,0) band at 398 nm, the DNA sample also contains external adducts, possibly a mixture of dG_{ext} and dA_{ext} adducts, as shown in the difference spectrum (Figure 6, a−b). The origin band for these adducts is located at 393.5 nm. The presence of this subpopulation is also shown in spectrum c, the temporal difference spectrum for fluorescence spectra acquired using two different detector delay times (0 and 50 ns). The broad fluorescence emission feature at 445 nm observed for the DNA sample was also present in the (±)-*anti*-DB[*a,l*]PDE−poly(dA)•poly(dT) sample and is due to excimer fluorescence from adducts bound to neighboring bases.

4. (±)-*syn*-DB[*a,l*]PDE Adducts with Polynucleotides and DNA. NLN fluorescence spectra of (±)-*syn*-DB[*a,l*]PDE adducts in double-stranded poly(dG)•poly(dC) acquired with two different excitation wavelengths are shown in Figure 7. Spectrum a was obtained using nonselective excitation at 308 nm, while spectrum b corresponds to intercalated adducts selectively excited at 370 nm. The difference spectrum (a − b) reveals adducts having an external conformation, which are less efficiently excited at 370 nm. The origin band for this fraction is located at 392.6 nm. A minor contribution from another adduct having an even more external character is observed at 382.5 nm.

Adducts from the reaction of (±)-*syn*-DB[*a,l*]PDE with poly(dA)•poly(dT) and with CT-DNA also exhibit both external and intercalated conformations, along with a contribution from excimer fluorescence at approximately 440 nm (spectra not shown). The results are summarized in Table 4 along with the spectral characteristics of all the adducts described above.

5. DB[*a,l*]P Adducts in Mouse Epidermis DNA. Figure 8 shows fluorescence spectra of mouse skin DNA

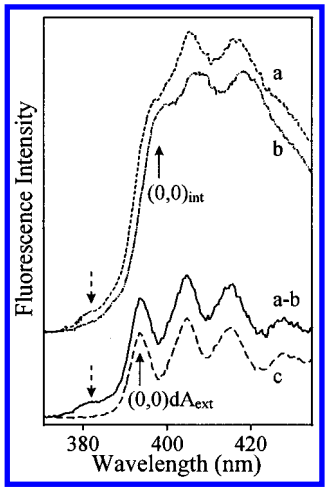

Figure 8. NLN fluorescence spectra (λ_{ex} = 360 nm, detector delay time 25 ns) of DNA from mouse skin epidermis obtained at two different time points after exposure to DB[*a*,*l*]P: 24 h (curve a) and 48 h (curve b). Spectrum a − b is the difference between spectra a and b, while curve c is the spectrum of the external *anti*-DB[*a*,*l*]PDE−dA [(±)-2] adduct observed in poly(dA)•poly(dT) oligonucleotide (same as Figure 6, curve (a − b).

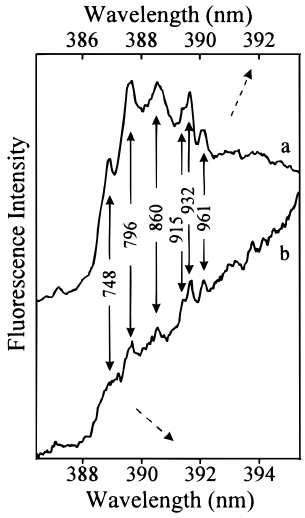

Figure 9. FLN spectra of *cis-anti*-DB[*a*,*l*]PDE−dAMP standard adduct (spectrum a) and the 24-h mouse skin DNA sample (spectrum b), obtained at 4.2 K for excitation wavelengths of 376.0 and 378.0 nm, respectively (see text). The FLN peaks are labeled with their S_1 excited-state vibrational frequencies, in cm^{-1}.

obtained at two different time points after exposure to DB[*a*,*l*]P, 24 h (Figure 8a) and 48 h (Figure 8b). The highest level of binding was detected 24 h after treatment; at 48 h the total adduct level had decreased as a result of DNA repair processes (see ^{32}P-postlabeling results). By comparing spectra a and b in Figure 8 measured under identical conditions, it is possible to determine which adduct conformation is being removed more efficiently. The difference spectrum (a − b) is almost identical to that for the external *anti*-DB[*a*,*l*]-PDE−dA adduct observed in poly(dA)•poly(dT) (Figure 5, a − b) but is different from those of the external (±)-*anti*-DB[*a*,*l*]PDE−dG, (±)-*syn*-DB[*a*,*l*]PDE−dG, and (±)-*syn*-DB[*a*,*l*]PDE−dA adducts. In addition to the external *anti*-dA adduct, there is a minor adduct (origin band at 382.5 nm, labeled by the dashed arrow in Figure 8) which is also removed in the 24−48-h time period. This band is not due to tetrol degradation (hydrolysis) products, since the fluorescence spectra of DB[*a*,*l*]P tetrols in the presence of DNA are red-shifted to ∼387 nm, due to physical complexation. This adduct most likely corresponds to a minor *trans-syn*-DB[*a*,*l*]PDE−dG adduct (see Discussion for details). In summary, these results show that the external adducts are preferentially removed in the time frame from 24 to 48 h.

To positively identify the efficiently repaired *anti*-DB-[*a*,*l*]PDE−dA_{ext} adduct fraction in mouse skin DNA, FLN spectra for the DNA samples and *trans*- and *cis-anti*-DB-[*a*,*l*]PDE mononucleotide−dAMP adduct standards have been acquired. There are significant differences in the vibrational frequencies between *trans-anti*-DB[*a*,*l*]PDE−dAMP and *cis-anti*-DB[*a*,*l*]PDE−dAMP adducts that enable spectral distinction between these two adducts.[2] There are characteristic modes at 348, 396, 860, 915, 932, and 960 cm^{-1} for the *cis-anti*-DB[*a*,*l*]PDE−dAMP[2] adduct, while *trans-anti*-DB[*a*,*l*]PDE−dAMP adduct has modes at 748, 773, 803, 842, and 926 cm^{-1}. A detailed comparison of FLN spectra obtained at different excitation wavelengths showed that only the FLN spectra of *cis-anti*-DB[*a*,*l*]PDE−dAMP featured the same vibrational frequencies as those observed for the mouse skin DNA samples. An example of FLN spectra for *cis-anti*-DB[*a*,*l*]PDE−dAMP [with (0,0) band at ∼390 nm] and mouse skin DNA [with (0,0) band at ∼392 nm] is shown in Figure 9, spectra a and b, respectively. These spectra were obtained with different excitation wavelengths (376.0 and 378.0 nm) in order to compensate for the shift of their respective fluorescence (0,0) origin bands (see Discussion). On the basis of the agreement of the vibrational frequencies in the FLN spectra shown in Figure 9, the efficiently repaired *anti*-dA_{ext} adducts formed in mouse skin DNA can be assigned as a *cis-anti*-DB[*a*,*l*]PDE−dA adduct, in an external conformation.

Discussion

Vibronic Intensity Distribution. Before discussing adduct heterogeneity, conformations, and repair, we would like to address the different vibronic intensity distributions observed in the NLN fluorescence spectra obtained for various DB[*a*,*l*]PDE-derived adducts. Different vibronic intensity distributions have previously been observed for stereoisomeric tetrols derived from *syn*- and *anti*-DB[*a*,*l*]PDE (*35*) and nucleoside−dA adducts.[2] For *cis-anti*- and *trans-syn*-DB[*a*,*l*]P tetrol, the (0,0) band is the strongest feature in the fluorescence spectrum. In contrast, *trans-anti*- and *cis-syn*-DB[*a*,*l*]P tetrol exhibit stronger long wavelength emission bands compared to their fluorescence origin bands. External dA adducts on a single-stranded poly(dA) chain also have relatively strong vibronic bands, as shown in Figure 3b. Apparently, there is an increased probability of transition from the excited electronic state to higher vibrational levels of the ground state, as indicated by intensified long wavelength emission bands. The differences observed arise most likely from the fact that some vibronic bands are forbidden in the Condon approximation but can derive their intensities through vibronic coupling (*38*, *39*). Thus, on the basis of the NLN spectra presented here, we conclude that also in the case of DB[*a*,*l*]PDE-derived DNA adducts (with B[*e*]P chromophore, C_{2V} symmetry)

[2] Devanesan, P. D., Ariese, F., Jankowiak, R., Small, G. J., Rogan, E. G., and Cavalieri, E. L. A novel method for the isolation and identification of stable DNA adducts of dibenzo[*a*,*l*]pyrene and dibenzo-[*a*,*l*]pyrene diol epoxide formed in vitro. *Chem. Res. Toxicol.*, submitted.

Table 5. Compilation of Adducts Observed in Mouse Skin DNA in Vivo from Animals Treated Topically with DB[*a,l*]P, Based on Laser-Excited Low-Temperature Fluorescence Spectroscopy

	DB[*a,l*]P (in vivo)		
carcinogen sample	adduct label	(0,0) band (nm)	adduct/conformation assignment
mouse skin DNA (24 h after exposure)	(±)-1	382.5	*trans-syn*-DB[*a,l*]PDE−dA_{ext} with possible contribution from *anti*-DB[*a,l*]PDE−dG_{ext} and/or *syn*-DB[*a,l*]PDE−dG_{ext}[a]
	(±)-2	393.4	*cis-anti*-DB[*a,l*]PDE−dA_{ext}
	(±)-3	398	mixture of dA_{int} and dG_{int} adducts, mostly from *anti*-DB[*a,l*]PDE[b]
	c	445	closely spaced (neighbored) *anti*-DB[*a,l*]PDE−dA_{ext}[d]

[a] Note that based on ^{32}P-postlabeling data the (±)-*syn*-DB[*a,l*]PDE−dG adduct is not formed in mouse skin and therefore it can be excluded; however, this adduct was observed in the rat liver microsomal reaction. *anti*-DB[*a,l*]PDE−dG_{ext} [(±)-1] with (0,0) band at 382.5 nm cannot be excluded, although it was not observed in in vitro studies, perhaps due to a small contamination by tetrols in the ∼386-nm region. [b] On the basis of ^{32}P-postlabeling results, we have shown that dA_{int} and dG_{int} adducts are major and minor, respectively. [c] External adducts presumably formed in "hot spots", which have runs of neighboring or closely spaced adenine bases. [d] A minor contribution from *syn*-DB[*a,l*]PDE−dA_{ext} cannot be excluded.

the vibronic intensity distribution is strongly conformation-dependent and is caused by vibronically induced mode mixing and conformationally induced symmetry changes (distortion from planarity). To interpret the spectroscopic results, however, it is enough to consider the wavelengths of the fluorescence (0,0) bands listed in Tables 4 and 5.

Multiple Adduct Conformations. Our key spectroscopic findings regarding (±)-*anti*- and (±)-*syn*-DB[*a,l*]-PDE-derived DNA and polynucleotide adducts, utilizing time-resolved spectroscopy and selective laser excitation, are in agreement with previous studies of B[*a*]P−DNA adducts which showed that adducts may exist in external and intercalated conformations (*20*). Detailed studies have shown that a strong interaction between the B[*a*]P chromophore and the DNA helix leads to a red shift and spectral broadening, while the spectra of mononucleotide adducts are blue-shifted and fairly sharp (*20*). Based on the extent of the red shift observed for the fluorescence origin band of the pyrenyl fluorescence spectrum and strength of the electron−phonon coupling, it has been shown that *anti*-B[*a*]PDE−DNA adducts can exist in helix-external [(±)-1], partially based-stacked [(±)-2], and intercalated [(±)-3] conformations (*20*). We have now found that DB[*a,l*]PDE-derived adducts also adopt multiple conformations. As in the case of B[*a*]PDE adducts, DB[*a,l*]PDE adducts will also be designated by (±)-1, (±)-2, and (±)-3, to denote their conformations. The convention adopted in our group is that the S_1 state energy (energy of the fluorescence origin band) decreases with increasing number associated with the (±)-adduct label. Alternatively, adducts have also been classified by other workers (*23*, *24*) as type I (intercalated), type II (external), or type II′ (external, with partial base stacking) (*33*). Thus, an adduct having its (0,0) band at ∼383 nm is assigned as (±)-1 [or type II according to Geacintov's terminology (*23*, *24*)], a second external adduct with (0,0) at ∼393 nm is (±)-2 (or type II′), and an intercalated adduct (origin band at 398 nm for *anti*- and at 399 nm for *syn*-DB[*a,l*]PDE adducts) is (±)-3 (or type I). Our terminology of adduct classification is used throughout this work. The observed large red shifts are caused by different $\pi-\pi$ interactions between an adduct and the DNA bases and also by conformational changes in the cyclohexenyl ring of the DB[*a,l*]PDE adducts (*33*, *36*).

(±)-*syn*-DB[*a,l*]PDE Adducts with Polynucleotides and CT-DNA. Adducts derived from *syn*-DB[*a,l*]PDE in double-stranded oligonucleotides and DNA exist in multiple conformations, as summarized in Table 4. In double-stranded poly(dG)•poly(dC), two different external conformations [(±)-2 and (±)-1] with origin bands located at 382.5 and 392.6 nm, respectively, are formed. Previous conformational studies, including molecular dynamics simulation and calculations of the UV transitions, of *syn*-DB[*a,l*]PDE-derived depurinating DNA adducts (*syn*-DB[*a,l*]PDE-N7Ade and *syn*-DB[*a,l*]PDE-N7Gua) have established that *trans-syn*-DB[*a,l*]PDE adducts with (0,0) bands at 382.5 nm correspond to a conformation in which the cyclohexenyl ring adopts a half-boat structure, with adenine or guanine in a pseudoaxial position and minimal stacking interaction between the DNA bases and the distal ring of DB[*a,l*]P (*36*). Therefore, the conformation of these (±)-1 adducts must correspond to an external configuration with the cyclohexenyl ring in a half-boat conformation and negligible interaction with the bases of the poly(dG)•poly(dC) oligonucleotide. The conformation of the (±)-2 adducts in poly(dG)•poly(dC), having their origin band shifted to ∼393 nm, although still external in nature, must be characterized by a significant base-stacking interaction. Red-shifted, presumably intercalated conformation [(±)-3] of *syn*-DB[*a,l*]PDE-derived adducts is also formed in poly(dG)•poly(dC), with its origin band at 399 nm. The reaction of *syn*-DB[*a,l*]-PDE with poly(dA)•poly(dT) and with CT-DNA in vitro results in the formation of external but base-stacked adducts [(±)-2] and intercalated adducts [(±)-3]. Although these samples do not possess the blue-shifted external (±)-1 conformation observed in poly(dG)•poly-(dC), they do exhibit broad-band excimer-type fluorescence at 440 nm that is not observed for the poly(dG)•poly-(dC) sample. Since this excimer fluorescence has been observed for poly(dA)•poly(dT) and DNA samples but not for poly(dG)•poly(dC), it is believed to be due to external adducts bound to neighboring adenine bases, presumably in an external configuration. Only this type of configuration could lead, in the excited state, to the observed excimer type fluorescence.

(±)-*anti*-DB[*a,l*]PDE Adducts with Polynucleotides and CT-DNA. It is important to note that the adduct yield with CT-DNA is approximately 8 fmol/μg of DNA for *anti*-DB[*a,l*]PDE and about 10-fold less for *syn*-DB[*a,l*]PDE. Adducts derived from *anti*-DB[*a,l*]PDE in double-stranded oligonucleotides and DNA also exist in multiple conformations, as summarized in Table 4. In this case, for double-stranded poly(dG)•poly(dC), an intercalated conformation is formed but only one external conformation [(±)-2), presumably in a half-boat conformation] is observed. No blue-shifted external (±)-1 conformation is observed in this case. The reaction of *anti*-DB[*a,l*]PDE with poly(dA)•poly(dT) and with DNA

leads to the formation of external base-stacked adducts [(±)-2] and intercalated adducts [(±)-3]. Excimer-type fluorescence is also observed for these samples at 445 nm [but not for poly(dG)•poly(dC)], consistent with the presumption that the excimer fluorescence originates from adducts bound to neighboring or closely spaced adenine bases in the poly(dA)•poly(dT) and DNA samples.

Conformations of External Adducts. The conformation of the *anti*-DB[*a*,*l*]PDE−dA adduct in single-stranded poly(dA), obtained by denaturing the poly(dA)•poly(dT) sample, is characterized as an external (±)-1 adduct. Its (0,0) band is located at 382.6 nm, as shown in Figure 3. Recent spectroscopic data obtained for the *trans-anti*-DB[*a*,*l*]PDE−dA mononucleotide showed that this adduct may exist in two different conformations, with (0,0) bands at 382.6 and 388.2 nm, respectively. Detailed characterization of dA adducts will be published separately. Other spectroscopic data, molecular modeling, and molecular dynamics simulations performed for *trans-anti*-DB[*a*,*l*]P tetrol (*35*) and preliminary calculations for the *trans-anti*-DB[*a*,*l*]PDE−dA adduct show that the cyclohexenyl ring of the dA adduct [as was the case for DB[*a*,*l*]P tetrol (*35*)] may exist in two different half-chair conformations. In the first conformation, the base substituent in the fjord region at the C14-position adopts a semiaxial position, while its orientation in the second conformation is semiequatorial. On the basis of these results and spectroscopic data presented in this paper, we conclude that the external dA adducts in single-stranded poly(dA) (origin band at 382.6 nm) differ from the external dA adducts in double-stranded poly(dA)•poly(dT) (origin band at 393.4 nm) in the conformation of the cyclohexenyl ring and the amount of stacking interaction with the DNA bases. Since other experimental studies show that only *trans-anti*-DB[*a*,*l*]P tetrols (*35*) (but not the *cis*-tetrols) undergo conformational changes in different solvent systems (*35*), we conclude, based on the data shown in Figure 3, that the intercalated dA adduct in poly(dA)•poly(dT) with (0,0) band at 398 nm [which yields the external dA adduct in single-stranded poly(dA) upon denaturation] is formed by a *trans* opening of the *anti*-diol epoxide. Therefore, the external (±)-2 adducts in poly(dA)•poly(dT) with origin band at 393.4 nm (Figure 8, spectrum c) must correspond to adducts formed by *cis* opening of the *anti*-diol epoxide. The presence of this adduct and its stereochemistry, in the case of mouse skin DNA, have been confirmed by FLN spectra shown in Figure 9.

The external dG adducts derived from (±)-*syn*-DB[*a*,*l*]PDE in poly(dG)•poly(dC) also exhibit two external conformations: (±)-1 and (±)-2 adduct types with their origin bands at 382.5 and 392.6 nm, respectively. In this case, on the basis of previous spectroscopic results and molecular dynamics simulations obtained for *trans-syn*-DB[*a*,*l*]P tetrols and depurinating *trans-syn*-DB[*a*,*l*]PDE-N7Gua and -N7Ade adducts (*36*), we believe that the band at 382.5 nm corresponds to a conformation in which the cyclohexenyl ring adopts a boatlike structure. Interestingly, only one external dA adduct type (base-stacked) with origin band at 392.5 nm is observed in poly(dA)•poly(dT) samples. This sample, however, shows a significant contribution of excimer-type fluorescence originating, presumably, from external type II adducts.

Sequence Specificity. Excimer-type fluorescence is observed not only for the in vitro modified poly(dA)•poly(dT) and DNA samples, which have high adduction levels, but also for the mouse skin DNA samples, obtained in vivo, that have a very low damage level. This is remarkable and seems to indicate that there may be cooperativity effects that lead to adduct formation on neighboring bases or that there may be regions of the DNA strand (hot spots) that are more susceptible to adduct formation on neighboring bases. It has been shown previously by Ross et al. (*40*) using the reaction of fjord region benzo[*c*]phenanthrene-3,4-diol 1,2-epoxides with a specific gene sequence (*supF* gene, 1 modification/200 base pairs) that individual stereoisomers of diol epoxides show a remarkable sequence specificity to produce a unique pattern of adduct hot spots.

Comparison of ^{32}P-Postlabeling and Fluorescence Results. Since the fluorescence results have been obtained for native, adducted DNA samples, while the ^{32}P-postlabeling results have been obtained for DNA samples digested to the 3′-nucleotide level, different information is obtained. The major DB[*a*,*l*]P−DNA adducts formed in mouse skin DNA in vivo, as determined by ^{32}P-postlabeling, are (−)-*anti*-DB[*a*,*l*]PDE−dA, (−)-*anti*-DB[*a*,*l*]PDE−dG, and (±)-*syn*-DB[*a*,*l*]PDE−dA (see Tables 1 and 2). Three of the major adducts (spots 1−3 in Figure 2B) account for ∼85% of the total stable adducts formed in mouse skin DNA. The results of laser-induced fluorescence spectroscopy (Table 5) indicate that the following adducts are formed in mouse skin: *anti*-DB[*a*,*l*]PDE−dA and −dG (intercalated trans-type adducts), *cis-anti*-DB[*a*,*l*]PDE−dA [external, (±)-2 adduct], and a minor external adduct, most likely (±)-*trans-syn*-DB[*a*,*l*]PDE−dA, that may also include a small contribution from (±)-*syn*-DB[*a*,*l*]PDE−dG.

The ^{32}P-postlabeling results indicate that in mouse skin DNA, *anti*-DB[*a*,*l*]PDE adducts originate from the (−)-enantiomer. This stereoselectivity is consistent with previous observations made for the activation of DB[*a*,*l*]P in MCF-7 cells (*5*) and mouse skin (*6*). The fluorescence data, while not providing information on chirality, yields information regarding the conformations of the adducts; external [(±)-1], external base-stacked [(±)-2], and intercalated [(±)-3] adducts all form in mouse skin DNA exposed to DB[*a*,*l*]P. On the basis of fluorescence spectroscopy and molecular modeling and dynamics simulations, the two major dA adducts derived from *anti*-DB[*a*,*l*]P diol epoxide (spots 2 and 3 in the ^{32}P-postlabeling results in Figure 2B) correspond to cis (origin band at 393.4 nm) and trans (origin band at 398 nm) addition, respectively. The ^{32}P-postlabeling and fluorescence results can also be combined to confirm or discount the formation of specific adducts. For instance, a possibility of a minor contribution from (±)-*syn*-DB[*a*,*l*]PDE−dG in mouse skin DNA, which could not be excluded based on the fluorescence data, can be rejected, since only (±)-*syn*-dA [not (±)-*syn*-dG] adducts were positively identified by ^{32}P-postlabeling.

Low-temperature fluorescence spectroscopy can differentiate between different conformations of DNA adducts and reveal differences in their repair rates. The analysis of mouse skin DNA samples obtained at 24 and 48 h after exposure to DB[*a*,*l*]P clearly shows that external adducts are repaired more efficiently than intercalated adducts. The structure of one of these adducts, *cis-anti*-DB[*a*,*l*]PDE−dA (spot 2, Figure 2B), an external (±)-2 type adduct, has been identified by FLN spectroscopy (Figure 9). A minor external (±)-1 type adduct, i.e., (±)-*trans-syn*-DB[*a*,*l*]PDE−dA (tentatively

assigned as spot 4 in the ^{32}P-postlabeling data in Figure 2B), is also preferentially repaired. The identity of this minor adduct (origin band at 382.5 nm in Figure 8) has been assigned based on spectroscopic and computational analysis of various DB[*a*,*l*]P diol epoxide adduct standards and their tetrol hydrolysis products. Thus the fluorescence results indicate that conformation-dependent repair of DB[*a*,*l*]P−DNA adducts occurs, as has been observed previously for mouse skin DNA exposed to B[*a*]P (*20*).

Conclusions

The present study has shown that the combination of ^{32}P-postlabeling and low-temperature fluorescence spectroscopy provides a powerful methodology for investigating the structures and conformations of DNA adducts, including adduct heterogeneity, persistence, and repair. The two methods are complementary and provide more insight into adduct formation and composition than either method alone can provide.

DB[*a*,*l*]P−DNA adducts that form in mouse skin exposed to DB[*a*,*l*]P are very heterogeneous, possessing different structures and different conformations. External [(±)-1 type], external but base-stacked [(±)-2], and intercalated [(±)-3] adduct conformations are all observed in mouse skin DNA samples. Based on the ^{32}P-postlabeling and fluorescence data, it can be estimated that the majority (approximately 75%) of the adducts formed in mouse skin DNA at 24 h adopt intercalated conformations that are less efficiently repaired than external adducts. Taken together with our recent data on B[*a*]P−DNA adducts (*20*), it seems that the DNA repair system differentiates between adduct structure and conformation in the process of repairing DNA damage resulting from PAH diol epoxides.

The finding that DB[*a*,*l*]PDE−dA adducts are the major adducts formed in mouse skin DNA in vivo is in agreement with an earlier study performed in MCF-7 cell cultures, where 80−90% of the adducts were attributed to adenine modification (*5*). In other studies the ratio of guanine to adenine adducts was nearer 1:1 (*41*). However in these studies, the first involving microsomal activation of the hydrocarbon and the second an analysis of adducts in mouse lung following ip injection, a significant proportion of the adducts were formed by the *syn*-diol epoxide. In mouse skin, however, the overwhelming majority of adducts are formed by the (−)-*anti*-diol epoxide (ref *6* and this study), which appears to show a greater selectivity for adenine residues. In the present study we detected only a small contribution to DNA binding (ca. 3%) by the *syn*-diol epoxides; an earlier study failed to detect any contribution by these isomers to DNA binding in mouse skin (*6*).

All studies indicate that stable DB[*a*,*l*]PDE−DNA adducts are formed in vivo by the metabolic activation of DB[*a*,*l*]P to the fjord region DB[*a*,*l*]P-11,12-diol 13,14-epoxides, which subsequently react with dA and dG residues presumably at the exocyclic amino groups, as has been demonstrated also for a variety of other PAH diol epoxides (*42*−*44*). In contrast, binding of DB[*a*,*l*]-PDE at the N7 positions of dA and dG has been shown to lead to depurination in vitro (*9*). Further studies on adduct composition, their repair, and mutational events caused by adducts derived from DB[*a*,*l*]P (via both monooxygenation and one-electron oxidation pathways) will be required to establish a correlation between mutations and the DB[*a*,*l*]P adduct structure involved.

Although fluorescence analysis was able to reveal differences in the relative rates of repair of adducts between 24 and 48 h, these were not evident from analysis by ^{32}P-postlabeling. The probable reasons for this are that the variations in quantitation inherent in this method are too great to detect small absolute differences in the percentage contributions of individual adduct spots to the total binding. Alternatively, the fact that the different repair rates are not reflected in the postlabeling spots is because several adducts may exist as both external (minor) and intercalated (major) conformations. Then, if for all these adducts some of the minor population is repaired more readily, the relative intensities of the adduct spots would still be more or less the same.

Nevertheless, the spectroscopic study presented in this manuscript indicates that a relatively high amount of DB[*a*,*l*]PDE−DNA adducts adopt intercalated conformations and are, therefore, more resistant to repair than external adducts. This may be one of the reasons that DB[*a*,*l*]P is the most potent PAH carcinogen presently known (*1*−*15*).

Acknowledgment. Ames Laboratory is operated for the U.S. Department of Energy by Iowa State University under Contract No. W-7405-Eng-82. This work was supported by the Office of Health and Environmental Research, Office of Energy Research, and the Deutsche Forschungsgemeinschaft SFB 302 (A.S.). Partial support to one of us (R.J.) from the International Union Against Cancer during the early stage of this project is also acknowledged. The authors thank Dr. E. L. Cavalieri and Dr. P. D. Devanesan (Eppley Institute for Research in Cancer, Omaha, NE) for providing us with the *trans-anti*- and *cis-anti*-DB[*a*,*l*]PDE−dAMP adduct standards.

References

(1) Cavalieri, E. L., Rogan, E. G., Higginbotham, S., Cremonesi, P., and Salmasi, S. (1989) Tumor initiating activity in mouse skin and carcinogenicity in rat mammary gland of dibenzo[*a*]pyrenes: the very potent environmental carcinogen dibenzo[*a*,*l*]pyrene. *J. Cancer Res. Clin. Oncol.* **115**, 67−72.

(2) Devanesan, P. D., Cremonesi, P., Nunnaly, J. E., Rogan, E. G., and Cavalieri, E. L. (1990) Metabolism and mutagenicity of dibenzo[*a*,*e*]pyrene and the very potent environmental carcinogen dibenzo[*a*,*l*]pyrene. *Chem. Res. Toxicol.* **3**, 550−586.

(3) Hughes, N. C., and Phillips, D. H. (1990) Covalent binding of dibenzopyrenes and benzo[*a*]pyrene to DNA: evidence for synergistic and inhibitory interactions when applied in combination to mouse skin. *Carcinogenesis* **11**, 1611−1619.

(4) Ralston, S. L., Lau, H. H. S., Seidel, A., Luch, A., Platt, K. L., and Baird, W. M. (1994) The potent carcinogen dibenzo[*a*,*l*]pyrene is metabolically activated to fjord-region 11,12-diol 13,14-epoxides in human mammary carcinoma MCF-7 cell cultures. *Cancer Res.* **54**, 887−890.

(5) Ralston, S. L., Seidel, A., Luch, A., Platt, K. L., and Baird, W. M. (1995) Stereoselective activation of dibenzo[*a*,*l*]pyrene to (−)-anti-(11*R*,12*S*,13*S*,14*R*)- and (+)-syn(11*S*,12*R*,13*S*,14*R*)-11,12-diol-13,-14-epoxides which bind extensively to deoxyadenosine residues of DNA in the human mammary carcinoma cell line MCF-7. *Carcinogenesis* **16**, 2899−2907.

(6) Ralston, S. L., Lau, H. H. S., Seidel, A., Luch, A., Platt, K. L., and Baird, W. M. (1994) Identification of dibenzo[*a*,*l*]pyrene-DNA adducts formed in cells in culture and in mouse skin. *Polycyclic Aromat. Compds.* **6**, 199−206.

(7) Cavalieri, E. L., Higginbotham, S., RamaKrishna, N. V. S., Devanesan, P. D., Todorovic, R., Rogan, E. G., and Salmasi, S. (1991) Comparative dose−response tumorigenicity studies of dibenzo[*a*,*l*]pyrene versus 7,12-dimethylbenz[*a*]anthracene, benzo-[*a*]pyrene, and two dibenzo[*a*,*l*]pyrene dihydrodiols in mouse skin and rat mammary gland. *Carcinogenesis* **12**, 1939−1944.

(8) Higginbotham, S., RamaKrishna, N. V. S., Johansson, S. L., Rogan, E. G., and Cavalieri, E. L. (1993) Tumor-initiating activity and carcinogenicity of dibenzo[*a*,*l*]pyrene versus 7,12-dimethyl-

benz[*a*]anthracene and benzo[*a*]pyrene at low dose in mouse skin. *Carcinogenesis* **14**, 875−878.
(9) Li, K.-M., Todorovic, R., Rogan, E. G., Cavalieri, E. L., Ariese, F., Suh, M., Jankowiak, R., and Small, G. J. (1995) Identification and quantitation of dibenzo[*a*,*l*]pyrene-DNA adducts formed by rat liver microsomes in vitro: preponderance of depurinating adducts. *Biochemistry* **34**, 8043−8049.
(10) Snook, M. E., Severson, R. F., Arrendale, R. F., Higman, H. C., and Chortyk, O. T. (1977) The identification of high molecular weight polynuclear aromatic hydrocarbons in a biologically active fraction of cigarette smoke condensate. *Beitr. Tabakforsch.* **9**, 79−101.
(11) Kozin, I. S., Gooijer, C., and Velthorst, N. H. (1995) Direct determination of dibenzo[*a*,*l*]pyrene in crude extracts of environmental samples by laser-excited Shpol'skii spectroscopy. *Anal. Chem.* **67**, 1623−1626.
(12) Luch, A., Glatt, H., Platt, K. L., Oesch, F., and Seidel, A. (1994) Synthesis and mutagenicity of the diastereomeric fjord-region 11,-12-dihydrodiol 13,14-epoxides of dibenzo[*a*,*l*]pyrene. *Carcinogenesis* **15**, 2507−2516.
(13) Gill, H. S., Kole, P. L., Wiley, J. C., Li, K.-M., Higginbotham, S., Rogan, E. G., and Cavalieri, E. L. (1994) Synthesis and tumor-initiating activity in mouse skin of dibenzo[*a*,*l*]pyrene *syn*- and *anti*-fjord-region diol epoxides. *Carcinogenesis* **15**, 2455−2460.
(14) Amin, S., Krzeminski, J., Rivenson, A., Kurtzke, C., Hecht, S. S., and Elbayoumy, K. (1995) Mammary carcinogenicity in female CD rats of fjord region diol epoxides of benzo[*c*]phenanthrene, benzo[*g*]chrysene and dibenzo[*a*,*l*]pyrene. *Carcinogenesis* **16**, 1971−1974.
(15) Amin, S., Desai, D., Dai, W., Harvey, R. G., and Hecht, S. S. (1995) Tumorigenicity in newborn mice of fjord region and other sterically hindered diol epoxides of benzo[*g*]chrysene, dibenzo[*a*,*l*]-pyrene (dibenzo[*def*,*p*]chrysene), 4H-cyclopenta[*def*]-chrysene and fluoranthene. *Carcinogenesis* **16**, 2813−2817.
(16) Chakravarti, D., Pelling, J. C., Cavalieri, E. L., and Rogan, E. G. (1995) Relating aromatic hydrocarbon-induced DNA adducts and c-H-ras mutations in mouse skin papillomas: the role of apurinic sites. *Proc. Natl. Acad. Sci. U.S.A.* **92**, 10422−10426.
(17) Melendez-Colon, V. J., Smith, C. A., Seidel, A., Luch, A., Platt, K. L., and Baird, W. M. (1997) Formation of stable adducts and absence of depurinating adducts upon reaction of the diol epoxides of the potent carcinogen dibenzo[*a*,*l*]pyrene with DNA in solution and in cells. *Proc. Natl. Acad. Sci. U.S.A.* **94**, 13542−13547.
(18) Choi, D.-J., Marino-Alessandri, D. J., Geacintov, N. E., and Scicchitano, D. A. (1994) Site-specific benzo[*a*]pyrene diol epoxide-DNA adducts inhibit transcription elongation by bacteriophase T7 RNA polymerase. *Biochemistry* **33**, 780−787.
(19) Tang, M., Pierce, J. R., Doisy, R. P., Nazimiec, M. E., and MacLeod, M. C. (1992) Differences and similarities in the repair of two benzo[*a*]pyrene diol epoxide isomers induced DNA adducts by *uvrA*, *uvrB*, and *uvrC* gene products. *Biochemistry* **31**, 8429−8436.
(20) Suh, M., Ariese, F., Small, G. J., Jankowiak, R. J., Hewer, A., and Phillips, D. H. (1995) Formation and persistence of benzo-[*a*]pyrene DNA adducts in mouse epidermis in vivo: importance of adduct conformation. *Carcinogenesis* **16**, 2561−2569.
(21) Singh, S. B., Hingerty, B. E., Singh, V. C., Greenberg, J. P., Geacintov, N. E., and Broyde, S. (1991) Structures of the (+)- and (−)-*trans*-*anti*-BPDE adducts to guanine-N^2 in a duplex dodecamer, *Cancer Res.* **51**, 3482−3492.
(22) Belguise-Valladier, P., and Fuchs, R. P. P. (1991) Strong sequence-dependent polymorphism in adduct-induced DNA structure: analysis of single N-2 acetylaminofluorene resides bound within the NaRI mutation hot spot. *Biochemistry* **30**, 10091−10100.
(23) Roche, C. J., Jeffrey, A. M., Mao, B., Alfano, A., Kim, S. K., Ibanez, V., and Geacintov, N. E. (1991) Dependence of conformations of benzo[*a*]pyrene diol epoxide-DNA adducts derived from stereoisomers of different tumorigenicities on base sequence. *Chem. Res. Toxicol.* **4**, 311−317.
(24) Cosman, M., Fiala, R., Hingerty, B. E., Armin, S., Geacintov, N. E., Broyde, S., and Patel, D. J. (1974) Solution conformation of the (+)-*cis*-*anti*-[BP]dG adduct opposite a deletion site in a DNA duplex: intercalation of the covalently attached benzo[*a*]pyrene into the helix with base displacement of the modified deoxyguanosine into the minor groove. *Biochemistry* **33**, 11518−11527.
(25) Drouin, E., and Loechler, E. L. (1993) AP sites are not significantly involved in mutagenesis by the (+)-anti diol epoxide of benzo[*a*]pyrene: the complexity of its mutagenic specificity is likely to arise from adduct conformational polyformism. *Biochemistry* **32**, 6555−6562.
(26) Rodriguez, H., and Loechler, E. L. (1993) Mutagenesis of the (+)-*anti*-diol epoxide of benzo[*a*]pyrene: what controls mutagenic specificity? *Biochemistry* **32**, 1759−1769.
(27) Jankowiak, R. (1992) Heterogeneous distribution and dispersive photodissociation rates of benzo[*a*]pyrene diol-epoxide enantiomer-DNA and -poly(dG-dC)•poly(dG-dC) adducts. *Biophys. Chem.* **42**, 133−146.
(28) Tierney, B., Hewer, A. H., Walsh, C., Grover, P. L., and Sims, P. (1977) The metabolic activation of 7-methylbenz[*a*]anthracene in mouse skin. *Chem.-Biol. Interact.* **18**, 179−183.
(29) Hughes, N. C., and Phillips, D. H. (1993) ^{32}P-Postlabeling analysis of the covalent binding of benzo[*ghi*]perylene to DNA in vivo and in vitro. *Carcinogenesis* **14**, 127−133.
(30) Gupta, R. C., Reddy, M. V., and Randerath, K. (1982) ^{32}P-Postlabeling analysis of nonradioactive carcinogen-DNA adducts. *Carcinogenesis* **3**, 1081−1092.
(31) Pfau, W., and Phillips, D. H. (1991) Improved reversed-phase high-performance liquid chromatographic separation of ^{32}P-labeled nucleoside 3′,5′-bisphosphate adducts of polycyclic hydrocarbons. *J. Chromatogr.* **570**, 65−76.
(32) Jankowiak, R., and Small, G. J. (1991) Fluorescence line narrowing: a high-resolution window on DNA and protein damage from chemical carcinogens. *Chem. Res. Toxicol.* **4**, 256−269.
(33) Suh, M., Ariese, F., Small, G. J., Jankowiak, R., Liu, T.-M., and Geacintov, N. E. (1995) Conformational studies of the (+)-*trans*, (−)-*trans*, (+)-*cis*, and (−)-*cis* adducts of *anti*-benzo[*a*]pyrene diol epoxide to N^2-dG in duplex oligonucleotides using polyacrylamide gel electrophoresis and low-temperature fluorescence spectroscopy. *Biophys. Chem.* **56**, 281−296 and references therein.
(34) Suh, M., Jankowiak, R., Ariese, F., and Small, G. J. (1994) Flanking base effects on the structural conformation of the (+)-*trans*-*anti*-BPDE adduct to N^2-dG in sequence-defined oligonucleotides. *Carcinogenesis* **15**, 2891−2898.
(35) Jankowiak, R., Ariese, F., Zamzow, D., Luch, A., Kroth, H., Seidel, A., and Small, G. J. (1997) Conformational studies of stereoisomer tetrols derived from *syn*- and *anti*-dibenzo[*a*,*l*]pyrene diol epoxides. *Chem. Res. Toxicol.* **10**, 677−686.
(36) Ariese, F., Small, G. J., and Jankowiak, R. (1996) Conformational studies of depurinating DNA adducts from *syn*-dibenzo[*a*,*l*]pyrene diol epoxide. *Carcinogenesis* **17**, 829−837.
(37) Li, K.-M., RamaKrishna, N. V. S., Padmavathi, N. S., Rogan, E. G., and Cavalieri, E. L. (1994) Synthesis and structure determination of the adducts of dibenzo[*a*,*l*]pyrene diol epoxides and deoxyadenosine and deoxyguanosine. *Polycyclic Aromat. Compds.* **6**, 207−213.
(38) Herzberg, G. (1966) Molecular spectra and molecular structure, III. *Electronic Spectra and Electronic Structure of Polyatomic Molecules*, Chapter II, van Nostrand and Reinhold Co., New York.
(39) Fisher, G. (1984) *Vibronic coupling. The interaction between the electronic and nuclear motions*, Chapters 3 and 4, Academic Press, New York.
(40) Ross, H., Bigger, C. A. H., Yagi, H., Jerina, D. M., and Dipple, A. (1993) Sequence specificity in the interaction of the four stereoisomeric benzo[*c*]phenanthrene dihydrodiol epoxides with the *supF* gene. *Cancer Res.* **53**, 1273−1277.
(41) Arif, J. M., and Gupta, R. C. (1997) Microsome mediated bioactivation of dibenzo[*a*,*l*]pyrene and identification of DNA adducts by ^{32}P-postlabeling. *Carcinogenesis* **18**, 1999−2007.
(42) Dipple, A., Pigott, M. A., Agarwal, S. K., Yagi, H., Sayer, J. M., and Jerina, D. M. (1987) Optically active benzo[*c*]phenanthrene diol epoxides bind extensively to adenine in DNA. *Nature* **327**, 535−536.
(43) Jerina, D. M., Chadha, A., Cheh, A. M., Schurdak, M. E., Wood, A. W., and Sayer, J. M. (1991) Covalent bonding of bay-region diol epoxides to nucleic acids. In *Biological Reactive Intermediates IV* (Witmer, C. M., Snyder, R., Jollow, D. J., Kalf, G. F., Koscis, J. J., and Sipes, I. G., Eds. pp 533−553, Plenum Press, New York.
(44) Dipple, A. (1994) Reactions of polycyclic aromatic hydrocarbons with DNA. In *DNA Adducts*: *Identification and Biological Significance* (Hemminki, K., Dipple, A., Shuker, D. E. G., Kadlubar, F. F., Segerbäck, D., and Bartsch, H., Eds. Vol. 125, pp 107−129, IARC Scientific Publications, Lyon.

TX970232K